Hydrol. Earth Syst. Sci. Discuss., 9, 337–378, 2012
www.hydrol-earth-syst-sci-discuss.net/9/337/2012/
doi:10.5194/hessd-9-337-2012

Hydrology and Earth System Sciences Discussions

Investigating patterns and controls of groundwater up-welling in a lowland river by combining fibre-optic distributed temperature sensing with observations of vertical head gradients

S. Krause[1,3], **T. Blume**[2], **and N. J. Cassidy**[3]

[1]School of Geographical, Earth and Environmental Sciences, University of Birmingham, Birmingham, UK
[2]Helmholtz Centre Potsdam, GFZ German Research Centre for Geosciences, Potsdam, Germany
[3]School of Physical and Geographical Sciences, Earth Science and Geography Department, Keele University, Keele, UK

Received: 24 November 2011 – Accepted: 5 December 2011 – Published: 10 January 2012

Correspondence to: S. Krause (s.krause@esci.keele.ac.uk)

Published by Copernicus Publications on behalf of the European Geosciences Union.

Abstract

This paper investigates the patterns and controls of aquifer-river exchange in a fast-flowing lowland river by the conjunctive use of streambed temperature anomalies identified with Fibre-optic Distributed Temperature Sensed (FO-DTS) and observations of vertical hydraulic gradients (VHG).

FO-DTS temperature traces along this lowland river reach reveal discrete patterns with "cold spots" indicating groundwater up-welling. In contrast to previous studies using FO-DTS for investigation of groundwater-surface water exchange, the fibre-optic cable in this study was buried in the streambed sediments, ensuring clear signals despite fast flow and high discharges. During the observed summer baseflow period, streambed temperatures in groundwater up-welling locations were found to be up to 1.5 °C lower than ambient streambed temperatures. Due to the high river flows the cold spots were sharp and distinctly localized without measurable impact on downstream surface water temperature.

VHG patterns along the stream reach were highly variable in space, revealing strong differences even at small scales. VHG patterns alone are indicators of both, structural heterogeneity of the stream bed as well as of the spatial heterogeneity of the groundwater-surface water exchange fluxes and are thus not conclusive in their interpretation. However, in combination with the high spatial resolution DTS data we were able to separate these two influences and clearly identify locations of enhanced exchange, while also obtaining information on the complex small-scale streambed transmissivity patterns responsible for the very discrete exchange patterns.

HESSD

9, 337–378, 2012

1 Introduction

1.1 Motivation: the importance of groundwater-surface water exchange at aquifer-river interfaces

Hydrological sciences have experienced a significant paradigm shift in recent years, advancing the rather static perception of rivers and aquifers as discrete entities towards a more complex and dynamic understanding of groundwater and surface water as integral components of a stream-catchment continuum (Bencala, 1993; Brunke and Gonser, 1997; Boulton et al., 1998; Boulton, 2007; Sophocleous, 2002; Krause et al., 2009a, 2011a; Woessner, 2000). The hyporheic zone (HZ), i.e. the interface between aquifer and river, plays a major role with respect to river ecohydrology and hydrochemistry (e.g. Malcolm et al., 2002, 2004; Stubbington et al., 2009; Robertson and Wood, 2010; Dole-Olivier et al., 1997; Malard et al., 2003; Fisher et al., 1998; Mulholland et al., 2000, 2008; Pinay et al., 2009; Krause et al., 2009b).

Reaction efficiency in hyporheic sediments is controlled by (i) the existence of steep redox-gradients and the availability of organic matter and microbial activity (Chafiq et al., 1999; Storey et al., 2004; Duff and Triska, 1990; Hinkle et al., 2001; Jones et al., 1995; Findlay et al., 1993, 2003; Fisher et al., 1998; Hill and Cardaci, 2004; Zarnetzke et al., 2011a) as well as (ii) hyporheic flow paths and residence times (Zarnetzke et al., 2011b; Fisher et al., 1998; Bencala et al., 1993; Duff and Triska, 2000; Jones et al., 1995). Hence, the assessment of the HZ functional importance with respect to water chemistry requires a detailed understanding of hyporheic exchange fluxes (White, 1993; Krause et al., 2011a).

Exchange fluxes over the aquifer-river interface are controlled (i) by hydraulic head gradients between groundwater and surface water as driving force and (ii) by the hydraulic conductivity of streambed sediments, which controls and limits the exchange. At the larger (up to several kilometre) stream reach to sub-catchment scale, exchange fluxes between groundwater and surface water can be strongly affected by larger geological heterogeneities in the alluvial aquifer and the resulting groundwater flow field

HESSD
9, 337–378, 2012

(Cardenas and Wilson, 2006; Fleckenstein et al., 2006; Engdahl et al., 2010; Frei et al., 2009). At smaller, plot to stream reach scales, however, exchange fluxes over the aquifer-river interface appear to be strongly controlled by spatial patterns of streambed hydraulic conductivity (Genereux et al., 2008; Leek et al., 2009; Calver, 2001; Rosenberry, 2008; Kaeser et al., 2009) and streambed geomorphology (Storey et al., 2003; Boano et al., 2006, 2010; Cardenas, 2009; Cardenas et al., 2008; Kasahara and Hill, 2008; Tonina and Buffington, 2007).

Although groundwater-surface water exchange fluxes have been subject to intensive investigation in the last two decades (e.g. Bencala, 1993; Cardenas et al., 2004; Cardenas and Wilson, 2006; Conant, 2004; Wondzell, 2006; Kasahara and Wondzell, 2003) the identification of spatial patterns and temporal dynamics of exchange fluxes between groundwater and surface water remains a challenge (White, 1993; Krause et al., 2011a).

A better understanding of streambed controls on aquifer-river exchange is particularly critical in lowland river systems where nutrient loads in groundwater and surface water are often increased as result of intensified agricultural management practice. HZ nutrient attenuation in lowland rivers has been shown to be substantial on the one hand while, as result of the complex depositional history of the river system, groundwater upwelling into the surface water often exhibits strong spatial heterogeneity on the other hand (Krause et al., 2008a,b).

As direct field measurements of groundwater-surface water exchange for instance by seepage meters (Rosenberry et al., 2008) are difficult, in particular in coarser streambed sediments (Rosenberry and Pitlick, 2009), vertical hydraulic gradients (VHGs) obtained from head observations in streambed piezometers have been widely used to describe the direction and magnitude of GW-SW fluxes (e.g. Krause et al., 2009b; Conant, 2004).

HESSD
9, 337–378, 2012

1.2 Heat as tracer for exchange fluxes at the aquifer-river interface

Several studies have demonstrated that temperature may be an efficient tracer for inferring groundwater- surface water interactions (e.g. Malcolm et al., 2002; Schmidt et al., 2007; Anibas et al.; 2009; Hannah et al., 2004, 2009; Constantz et al., 2003; Cardenas and Wilson, 2007; Krause et al., 2011b).

Streambed heat transfer is controlled by three processes; (i) advective heat transfer, (ii) conductive heat transfer and (iii) radiative heat transfer (Constantz, 2008; Hannah et al., 2004; Webb et al., 2008). Streambed temperature patterns have been frequently reported to be dominantly controlled by advective heat fluxes from down-welling surface waters or up-welling groundwater (Cardenas and Wilson, 2007; Hannah et al., 2004; Malcolm et al., 2002). By measuring streambed temperatures in an environment with significant differences in groundwater and surface water temperatures, the propagation of a heat signal can be used as proxy, indicating exchange flow directions (Hatch et al., 2010; Keery et al., 2007; Anibas et al., 2009; Schmidt et al., 2007; Anderson, 2005) or even to quantify exchange fluxes (Hatch et al., 2010; Westhoff et al., 2007).

The great advantages of temperature tracing methods are the relatively low costs and robust design of sensor technology. In particular the recent introduction of Fibre-optic Distributed Temperature Sensor (FO-DTS) networks into hydrology (Selker et al., 2006a,b; Selker, 2008; Tyler et al., 2007) has helped to significantly increase the spatial and temporal scale of temperature observations.

With one exception (Lowry et al., 2007) previous FO-DTS applications usually deployed the fibre-optic cable directly on top of the streambed surface (Selker et al., 2006a,b; Tyler et al., 2009; Westhoff et al., 2007; Slater et al., 2010). Therefore, temperatures measured along the fibre-optic cable did not directly reflect streambed pore-water temperatures but temperatures at the bottom of the surface water column. As the majority of previous FO-DTS studies for identification of aquifer-river exchange fluxes focused on smaller headwater streams, relative groundwater contributions in these environments were large enough to cause measurable in temperatures at the

HESSD
9, 337–378, 2012

bottom of the surface water column (e.g. Selker et al., 2006; Westhoff et al., 2007), often causing a change in stream temperature even downstream of the groundwater input. This leads to a stream temperature profile looking more like a step function instead of showing single localized spikes. FO-DTS applications for identification of groundwater-surface water exchange flow patterns in more lowland settings and larger streams, where relative groundwater contributions are smaller and therefore less likely to cause measurable changes in surface water temperatures, are limited in number (Lowry et al., 2007; Slater et al., 2010).

1.3 Aims and objectives

The applicability of VHG observations for predicting groundwater-surface water exchange flow patterns is limited as VHGs indicate pressure distributions only and a quantification of fluxes would also require consideration of sediment hydraulic conductivities (Kaeser et al., 2009). This presents a particular challenge in lowland rivers with complex patterns and wide ranges of streambed hydraulic conductivities. Furthermore, the VHG signal provides information on both forces and controls of aquifer-river exchange that are hard to discriminate. High VHG for instance can be caused by (i) regionally strong groundwater up-welling or (ii) local up-welling inhibition by streambed sediments of low hydraulic conductivity above the piezometer screen section.

FO-DTS monitored streambed temperatures on the other hand can provide a powerful indicator for patterns in groundwater-surface water exchange, in particular when a buried fibre-optic cable allows the direct measurement of streambed temperatures (Lowry et al., 2007). Although observed streambed temperature anomalies may be used to identify aquifer-river exchange flow patterns, they do not provide any information on the controls of the observed exchange flow patterns.

The objective of this study is to analyze the suitability of comparative analyses of FO-DTS derived temperature observations and piezometer VHG observations for identifying spatial patterns and temporal dynamics of aquifer-river exchange fluxes at an exemplary lowland river. It therefore aims to (i) identify actual exchange flow patterns

HESSD
9, 337–378, 2012

at the aquifer-river interface, (ii) combine DTS and VHG observations within a methodological framework that supports the analysis of process inference (specifically drivers and controls of aquifer-river exchange) and (iii) test the validity of framework inferred controls by comparison with streambed structural information.

2 Materials and methods

2.1 Study area

The study focuses on an approximately 300 m long meandering stream section of the River Tern (2°53′ W, 52°86′ N) (Fig. 1a). The field site extends into the immediate floodplain on both sides of the river (Fig. 1b). The wider research area was the subject of previous intensive investigations. It was selected by the UK Natural Environment Research Council (NERC) to represent characteristic lowland conditions within the Lowland Catchment Research Programme (LOCAR; Wheater and Peach, 2004). The local geology is dominated by the Permo-Triassic Sherwood Sandstone (PTS) formation, which forms one of the UK's major groundwater aquifers. The PTS is overlain by drift deposits of variable depth and hydraulic conductivities. Land use in the research area is dominated by pasture, with arable cereals and root crops grown in the area directly up-stream from the field site. The mean annual precipitation at the field site is 583 mm. Mean daily air temperature ranges from 3.7 °C (January) to 15.8 °C (July), with long-term (1957–2007) mean annual temperatures of 9.3 °C (Hannah et al., 2009). Mean river discharge at the Environment Agency operated Tern Hill (2°55′12″ W, 52°87′92″ N) gauging station (basin area 92 km^2, elevation 62 m a.s.l.) is 0.9 $m^3 s^{-1}$ with a 95 % exceedance (Q_{95}) of 0.4 $m^3 s^{-1}$ and a 10 % exceedance (Q_{10}) of 13.9 $m^3 s^{-1}$ (data period 1961–1990, UK National River Flow Archive, http://nwl.ac.uk/ih/nrfa). Summer baseflow conditions usually occur from May to October. The 5–8 m wide channel is limited by steep, on average 2 m high river

HESSD
9, 337–378, 2012

banks and includes a succession of pool-riffle-pool sequences mainly in the middle section (Krause et al., 2011b).

Sediment cores taken from the streambed (Fig. 1b) revealed substantial spatial sediment heterogeneity. Figure 2 shows two exemplary streambed cores that are representative for the sediment conditions in the investigated stream section. Whilst streambed sediments generally varied from mid-sized gravels to fine silty material with hydraulic conductivities (identified based on grain size distributions) typically in the range of 10^{-3}–10^{-5} m s^{-1} (as represented by core CI – Fig. 2), hydraulically, the most significant difference in streambed material was represented by the existence/absence of clay and peat layers of generally lower hydraulic conductivity (10^{-8}–10^{-9} m s^{-1}) as indicated in core CII (Fig. 2). The thickness and depth of the peat or clay structures within the streambed varied but did not exceed a thickness of 30 cm and during piezometer installation no peat or clay structures were found below streambed depths of 120 cm Streambed peat or clay structures are common in lowland rivers (Krause et al., 2007). With hydraulic conductivities in the range of 10^{-8} m s^{-1}, flow through these sediments is significantly reduced, potentially causing flow confinement and increased streambed residence times for up-welling groundwater (Fig. 2).

2.2 Experimental infrastructure

Field data were collected between June 2009–September 2010 with groundwater, surface water, interstitial pore water and air temperature as well as hydraulic heads in groundwater, surface water and streambed interstitial pore water being recorded (Table 1). Meteorological data were recorded at the nearby Keele meteorological station (52°59′55.86″ N; 2°16′12.90″ W). For observation of the shallow riparian groundwater within the floodplain drift deposits, ten 3 m deep groundwater boreholes were installed at the field site in 2008 (Fig. 1b). Three of the groundwater boreholes (GW1, GW3, GW7, Fig. 1b) and two river-stage gauging stations (SW1, SW3, Fig. 1b) were instrumented with pressure transducers to monitor both surface water and groundwater head (i.e. water depth) at 5–15 min intervals (Table 1). Monitored groundwater and surface

HESSD
9, 337–378, 2012

water pressure heads were corrected for barometric pressure fluctuations using an atmospheric pressure sensor located at groundwater borehole site GW 7 (Fig. 1b). Differential GPS was used for measuring the exact elevations of the installed boreholes and piezometers.

PTFE streambed piezometers comprising a central tube (12 mm inner diameter with 10 cm bottom screening section) for observations of interstitial pore water heads and up to seven tubes (1 mm inner diameter) for sampling of pore water profiles (Fig. 3a) were installed to depths of 150 cm within the streambed in 2008 (Figs. 1b and 3a). This setup allows for the investigation of aquifer-river exchange flow but does not account for very superficial (top cm) near-surface exchange fluxes. The piezometers were set up along a longitudinal transect along the stream reach with several cross-sectional extensions towards the river banks (Fig. 1). Hydraulic heads in streambed piezometers were monitored manually on seven sampling dates between 25 May 2009 and 30 September 2009 (Table 1), using an electric contact meter (dip-meter). Manual dip-meter measurements also covered the network of shallow riparian groundwater boreholes to provide quality assurance for the automatically logged pressure heads.

A fibre-optic Distributed Temperature Sensor network was employed for investigation of the streambed temperature patterns in response to aquifer-river exchange fluxes. FO-DTS uses the temperature dependent backscatter properties of a laser signal that propagates through a fibre-optic cable (Selker et al., 2006a,b; Tyler et al., 2009). The FO-DTS method applied in this project uses the offset in the backscatter of Raman stokes (temperature independent) and anti-stokes (temperature dependent) signals from a 10 nanosecond light pulse to undertake and locate temperature measurements along the fibre-optic cable (Selker et al., 2006a,b). The applied FO-DTS system (Sensornet Halo, Table 1) is capable of measuring temperature at high precision (0.05 °C) and with a spatial resolution of 2 m (Sensornet, 2009).

For the temperature survey a metal-armored two channel fibre-optic cable (BruSteel, Brugg/CH) was deployed. In most DTS studies (except Lowry et al., 2007), the cable has been deployed *on* the streambed, resulting in measurements of temperature at

HESSD
9, 337–378, 2012

the bottom of the surface water column. In contrast, in this study the fibre-optic cable was installed at an average depth of 5 cm within the streambed in order to directly measure streambed temperature and avoid signal loss due to advective lateral heat transport at the streambed surface caused by river flow. By ensuring careful installation of the cable along a longitudinal succession of shallow cuts into the streambed, variations in the depth of the deployed cable were assumed to be less than ±2.5 cm and disturbance of the streambed sediments was minimized. The cable was secured by approx. 100 tent pegs attached to the fibre-optic cable with plastic cable ties to avoid preferential heat conduction along the metal pegs. Introduced temperature variability as a result of spatially variable heat conduction and shallow hyporheic exchange into the sediment is small, according to previous investigations in the research area, with a maximum of 0.2–0.3 °C (Krause et al., 2011b). To match the spatial extent of the streambed VHG observations along the streambed piezometer network, the fibre-optic cable was deployed along a 500 m loop, covering both sides of the streambed (Fig. 3). Measurements were taken in double ended mode at 10 s intervals.

In order to calculate temperature offset and losses along the cable, sections of both cable ends were calibrated in temperature controlled warm/cold baths, allowing for a dynamic FO-DTS calibration. FO-DTS streambed temperature surveys were carried out during six days between 3 August 2009–19 August 2009 (Table 1), and comprised at least 100 double-ended measurements for each survey.

For the identification and monitoring of background temperatures in the groundwater and surface water, thermistors integrated in the water level pressure transducers measured temperatures at 5 to 15 min intervals (Fig. 1, Table 1). Additionally, reference measurements of streambed temperature were carried out at 15-min intervals by streambed thermistors installed at 5 and 10 cm depths along a pool-riffle pool succession at section P13-22 (Fig. 7, Krause et al., 2011b).

The combination of DTS-derived streambed temperatures and VHG observations at streambed piezometers is then used to provide a framework of case-distinctions of groundwater-surface water exchange fluxes in response to variability in streambed

HESSD
9, 337–378, 2012

hydraulic conductivity, in particular caused by the presence/absence of flow-confining streambed strata. A complete physical characterization of the highly heterogeneous streambed sediments for validation of presence or absence of low conductive streambed strata would have not been possible without complete disturbance of the in-situ sampling conditions. Therefore, assumptions regarding the presence of flow confining strata at piezometer locations were validated by using the sampling behavior of the mini-sampling tubes installed at approximately 20 cm intervals along the length of the piezometers. Pore-water sampling was inhibited if the sampling tube was located within low conductivity clay/peat lenses.

2.3 Data analysis

Vertical hydraulic gradients (VHG), indicating the strength and direction of exchange fluxes between groundwater and surface water, were determined from hydraulic head measurements in the streambed. VHG were calculated by $\Delta h/\Delta l$, with Δh given by the elevation difference of the water table observed inside and the stream stage outside the piezometer and Δl given by the distance between the mid-screen depth and the surface water-sediment interface. The accuracy of dip-meter based hydraulic head observations was approximately ±3 mm head and accounts for uncertainties in the measurements introduced by turbulent flow conditions around the piezometers, which can affect the outside head estimates (Krause et al., 2009b; Kaeser et al., 2009).

The analysis of the DTS data focused on the determination of temperature anomalies along the trace of the cable. Using the difference to the spatial average temperature of the cable as an indicator of the *strength of the temperature anomaly* (A_T) allows to compare anomalies on different dates independent of general (global) shifts in sediment temperatures and thus, provides a measure of the temporal variability of these signals (Eq. 1).

$$A_T(x_i) = T(x_i) - \overline{(T(x_i))} \quad (1)$$

x_i = measurement locations along the cable.

HESSD
9, 337–378, 2012

As this study focuses on a strongly gaining lowland river during summer, when groundwater temperatures are lower than in surface water, mainly negative temperature anomalies have to be expected as result of cold groundwater inputs. Anomaly strength is expected to vary with (a) changes in hydraulic gradients and thus changes in water fluxes and (b) changes in temperature gradients. A similar analysis was carried out for the vertical hydraulic gradients, compensating for overall (global) shifts in hydraulic gradients and thus, allowing for quantification and comparison of the *strength of VHG anomalies* (A_{VHG}) (Eq. 2).

$$A_{\mathrm{VGH}}\,(x_i) \;=\; \mathrm{VGH}\,(x_i) \;-\; \overline{(\mathrm{VGH}\,(x_i))} \tag{2}$$

x_i = locations of the piezometers.

The *variability of temperature and VHG anomalies* $A_T(x_i)$ and $A_{\mathrm{VHG}}(x_i)$ is described by their temporal *standard deviation* (sd) (Eq. 3):

$$\mathrm{sd}(A_T(x_i)) \;=\; \sqrt{\frac{1}{N}\sum_{t=1}^{N}\left(A_T(x_{it}) \;-\; \overline{A_T(x_i)}\right)^2}. \tag{3}$$

3 Results

3.1 Hydroclimatological conditions

Air temperatures varied by more than 20 °C during the observation period with $T_{\mathrm{max}} = 26.3$ °C, $T_{\mathrm{min}} = 5.6$ °C and the average = 15.2 °C (Fig. 4a). Diurnal air temperature amplitudes varied substantially with maximum day-night temperature differences of up to 14 °C in June and July. Although generally low in precipitation, the observation period included an extended wet period during July and early August (Fig. 4b). The summer baseflow period, with daily discharge ranging between 0.7–0.8 $\mathrm{m^3\,s^{-1}}$, was interrupted by a major discharge event with $Q > 1.5\,\mathrm{m^3\,s^{-1}}$ and >20 days with discharges >1.0 $\mathrm{m^3\,s^{-1}}$ resulting from the prolonged wet conditions in July 2009. Although

HESSD
9, 337–378, 2012

the runoff regime is mainly groundwater driven, a couple of rainfall events caused very immediate reactions in river discharge (e.g. during early June – see Fig. 4b). As the fibre-optic cable was installed during 30–31 July 2009 directly after the peak flow event and stream discharge quickly receded in August 2009, significant sediment shift during the FO-DTS survey can be excluded.

3.2 Riparian groundwater-surface water head patterns

Water levels at representative riparian groundwater boreholes (GW1, GW3, GW7) and river gauges (SW3) (see Fig. 1) were generally low during the baseflow conditions, only interrupted by a three-week episode of increased groundwater and surface water levels in July 2009 (Fig. 5a), caused by the increased precipitation events (Fig. 4a). Throughout most of the monitoring period, water levels in the groundwater boreholes (Fig. 1) exceeded surface water levels, indicating a general flow direction towards the stream. Inverse head gradients (indicating reversed flow conditions) were only observed during storm events (Fig. 4) when surface water levels rose faster and higher than the associated groundwater levels (Fig. 5a), causing surface water infiltration into the riparian groundwater.

3.3 Groundwater and surface water temperature patterns

Surface water temperature varied by more than 10 °C with $T_{min} = 11.7$ °C and $T_{max} = 22.2$ °C, whilst the range of temperature variations observed in the four groundwater boreholes (including also GW2, Figs. 1 and 5b) during the monitoring period was lower, i.e. 3.7 °C ($T_{min} = 9.4$ °C, $T_{max} = 13.1$ °C). The temporal dynamics of the stream temperatures strongly followed air temperature patterns (Fig. 2), with maximums in June and July. In contrast, groundwater temperatures were highest in August and September, indicating a several-week time lag in response to surface water/atmospheric conditions (Figs. 4 and 5b).

HESSD
9, 337–378, 2012

The described differences in temperature patterns produce strong thermal gradients between the groundwater and surface water (Fig. 5b). From June to August, surface water temperatures were up to 9.0 °C (average 3.1 °C) higher than groundwater temperatures. Towards the end of the observation period in September, differences between the groundwater and surface water temperatures became less distinct. During this period, the direction of groundwater-surface water temperature gradients changed at several occasions (Fig. 5b).

In a similar fashion to the air temperatures (Fig. 4a), diurnal temperature amplitudes in the surface water were clearly pronounced with ranges of up to 2.4 °C in June and July, but decreasing to below 1.0 °C in September (Fig. 5b). In contrast, groundwater temperatures exhibited no clear diurnal periodicity. Maximum daily changes in groundwater temperatures were below 0.2 °C. Even taking into account the up to 2.4 °C diurnal surface water temperature amplitudes, thermal gradients between groundwater and surface water exceeded 5 °C most of the time.

3.4 Spatial patterns of vertical hydraulic gradients and DTS temperatures

Vertical hydraulic gradients (VHG) at all 28 streambed piezometers were positive throughout the monitoring period (7 sampling dates during summer 2009), indicating groundwater up-welling into the river (Fig. 6). Observed VHG were spatially variable with values ranging from 0 (indicating hydraulic heads at the piezometer equal to the hydrostatic pressure of the stream and no up- or down-welling) to 0.92 (Fig. 6). At the most up-stream and down-stream sections in the North (P1–3) and the South end (P25–27) of the meander, VHG were low to moderate with 0.20–0.30 (average 0.26) whilst the Northwest-Southeast oriented central part (P4–24) of the meander section was characterised by higher VHG ranges. Although spatial averages of VHG were quite similar in both sections (P4–12 = 0.30 and P13–24 = 0.32), the spatial variation of observed VHG over the more downstream section P13–24 exceeded with an range of 0.03–0.57 the observed range of VHG over the more up-stream section P4–12 (0.19–0.47).

HESSD
9, 337–378, 2012

Fibre-optic Distributed Temperature surveys were carried out on six occasions in July and August 2009. Figure 7 shows the temperature data mapped onto the river reach (4 temperature traces averaged over 20 s on different dates). Distinctive cold spots with streambed temperatures of up to 2 °C below the spatial average were found close to both ends (P1–4, P25–27) of the investigated reach as well as around piezometer locations P8 and P12 (compare Fig. 6). Although the range of streambed temperature variation was larger for the first two observation dates (3 August 2009, 6 August 2009), the location and spatial extent of the observed cold spots remained stable throughout the FO-DTS-monitoring dates (Fig. 7).

3.5 Temporal dynamics of spatial patterns (signal stability)

While VHG and DTS temperatures showed distinct spatial patterns for each snapshot sampling, hydraulic gradients and temperatures at each sampling point also exhibited considerable temporal variability. To investigate the temporal stability of the overall spatial patterns we analysed the strength and persistence of "anomalies" $A_T(x_i)$ and $A_{\mathrm{VHG}}(x_i)$ (see Sect. 2.3) to identify locations with signals that were significantly different to the average characteristics of the stream reach.

Figure 8a shows boxplot distributions of VHG anomalies ($A_{\mathrm{VHG}}(x_i)$), i.e. the difference from the spatial average of each sampling date for each of the monitored piezometers (Eq. 2). This allowed the identification of (a) locations with generally higher/lower than average gradients over all sampling dates and (b) locations showing more/less variability in time than the average. While VHGs at locations P4, P8, P12, P15, P18, P19, P22 and P23 were distinctly and persistently higher than average gradients, we also find locations where gradients are distinctly lower than average for all sampling dates (P6, P7, P11, P13, P14, P16, P17, P20 and P27). VHGs in the upstream and downstream sections (P1–3; P25–27) were generally quite close to the spatial mean (anomaly ≈0).

The analysis of the strength of temperature anomalies $A_T(x_i)$ based on FO-DTS observations (Fig. 8b) confirmed the heterogeneous temperature patterns in the

HESSD
9, 337–378, 2012

streambed with a spatial temperature variability of up to 2.3 °C. In addition to common temperature variations of ±0.4 °C around the spatial average, the boxplots also identified more substantial, temporally persistent cold spots with temperatures up to 1.8 °C colder than the spatial average.

In order to analyse the temporal variability in the observed spatial patterns of temperature and VHGs, the temporal mean and standard deviation (STDEV) of anomaly strength of both VHG and temperature where compared (Fig. 9). This allows for the testing of signal variability and robustness at locations where the temperatures or VHG differ strongly from the spatial average. The analysis is based on six FO-DTS temperature surveys and seven VHG observation dates (Table 1). STDEV for temperature anomalies varied between 0.02 and 0.51. For VHGs the STDEV varied between 0.01 and 0.26 over all measurement locations.

While the relationship between STDEV and mean temperature anomalies exhibits a negative correlation with a spearman correlation coefficient of −0.78 (Fig. 9a), it is slightly positively correlated for the VHGs (Fig. 9b) with a spearman correlation coefficient of 0.47. The STDEV of temperature anomalies are higher (ranging from 0.12–0.51) at locations with strong anomalies whereas at locations where temperatures are higher than the spatial average (anomaly >0), the STDEV values ranged from 0.02 to 0.20 (Fig. 9a). For locations with negative VHG anomalies, STDEVs were as low as 0.01–0.14 but reached levels up to 0.025–0.26 at locations with positive VHG anomalies (Fig. 9b).

Higher STDEV (Fig. 9e) observed at locations with strong negative anomalies in temperature (Fig. 9c) indicate that these locations (cold spots) also exhibit more intense temporal signal variability than locations where temperatures differ less from the spatial average. VHG locations with negative anomalies (Fig. 9d) show less temporal variability (Fig. 9f), whilst at locations with positive anomalies they are more variable in time, i.e. the VHG signal at high VHG locations varies more than at locations with low VHGs. Locations of lowest STDEV in VHG anomalies (Fig. 9f) coincided with areas of highest STDEV in DTS anomalies (Fig. 9e).

HESSD
9, 337–378, 2012

3.6 Streambed structural information

Even though it was not possible to retrieve sediment cores for validation to the depth of installation for all piezometer locations, the multi-level mini-piezometers design (Fig. 3a) made an approximate estimation of flow confining peat and clay layers possible. While their small diameter (1 mm) prevented direct VHG observations at the sampling tubes bundled up around the 150 cm deep central head observation tube with outlets at 15–20 cm vertical intervals (Fig. 3), low conductivity streambed zones could nevertheless be identified at 8 sampling locations where no pore water could be extracted (Table 2). Tests at selected locations such as CI and CII (Fig. 1) confirmed that inhibited pore water extraction at piezometer sampling tubes coincided with streambed peat or clay layers.

4 Discussion

4.1 Analysis of aquifer-river connectivity by hydraulic head gradients

Groundwater levels in the observation area generally exceeded surface water levels (Fig. 5a), indicating groundwater flow towards the river. Inverse head gradients (surface water heads greater than groundwater heads), indicating surface water infiltration into the riparian groundwater, were limited to episodic storm events (Fig. 5a). The observed spatial variability in groundwater heads may result from spatially variable groundwater fluxes or heterogeneity in the hydraulic conductivities of riparian sediments, which varied by 5 orders of magnitude from highly conductive sands to low conductive clay (see Sect. 2.1). Groundwater and surface water responses to storm events (e.g. end of July 2009 – Fig. 4b) differ in intensity and timing. In comparison to surface water, peaks in groundwater hydraulic heads are slightly delayed. Furthermore, peaks in groundwater heads exhibit a slower recession than in the surface water heads (Fig. 5a), which can be interpreted as the effect of retention by riparian storage.

HESSD
9, 337–378, 2012

The complex spatial patterns of observed VHGs in the research area (Fig. 6) could be interpreted as high spatial heterogeneity in groundwater up-welling. However, it is not possible to directly infer fluxes from VHG observations as in streambeds with spatially highly variable hydraulic conductivities VHGs have been found to be poor indicators of groundwater – surface water exchange (Kaeser et al., 2009). It is, therefore, not possible to discriminate whether VHG patterns result from spatial variability in groundwater flow or hydraulic conductivities (Fig. 2) without further detailed knowledge on the physical aquifer and streambed properties.

It is unlikely that the observed high VHG values indicate intensive groundwater up-welling induced by spatial heterogeneity in the regional groundwater flow as caused by faults or fissures in the bedrock, for instance, as the geological properties of the non-fractured Permo-Triassic sandstone aquifer at the research area are spatially very homogeneous. However, the streambed cores revealed substantial variability in the physical properties of the near-surface materials including hydraulic conductivities (Fig. 2). The spatially isolated high VHG values of up to 0.6 (as seen in the central stream section) can be interpreted as indicators of the local inhibition of groundwater up-welling caused by the presence of flow confining streambed peat and clay lenses. At locations with lower (0.05–0.2) and spatially more homogeneous VHGs (i.e. the most up-stream and down-stream sections – P1–3 + P25–27; Fig. 6) this degree of flow inhibition is less likely.

High temporal variability ranges of VHG anomalies $A_{\mathrm{VHG}}(x_i)$ in the central river section (Fig. 8a) could be interpreted as an increased susceptibility of VHG to meteorologically-induced changes in larger-scale groundwater-surface water head ratios when flow confining streambed structures are present. In highly conductive sediments, when surface water heads react faster to storm events than groundwater heads, the resulting alteration of head differences between groundwater and surface water can be quickly equilibrated by exchange fluxes over the aquifer-river interface. Underneath flow confining streambed structures, however, flood-induced alteration of VHG anomalies would be more persistent as exchange between the groundwater and surface

HESSD
9, 337–378, 2012

waters (and resulting head equilibration) would be inhibited. Any increased temporal variability in VHG anomalies could, therefore, be interpreted as further indication of flow confining conditions, whereas temporally stable VHG anomalies (as in the most up-stream and most down-stream sections, Fig. 8a) could indicate highly conductive streambed sediments where groundwater-surface water head differences are faster equilibrated by exchange fluxes.

Nevertheless, without further detailed knowledge of the hydraulic conductivity patterns of the streambed sediments the above interpretations remain hypothetical, representing a particular limitation for VHG interpretations in structurally complex streambed environments. Table 2 confirms that VHG above the spatial average in many cases coincide with the observation of flow confining layers, indicating that high head gradients result from local inhibition of the groundwater up-welling. However, at other locations (e.g. P4, P8, P12, P20) this is not the case. High VHG at these piezometers adjacent to confined areas might indicate preferential pressure releases along intersecting flow paths resulting in locally intensified groundwater up-welling. A confirmation of these assumptions requires further information on actual groundwater up-welling patterns.

4.2 Identification of groundwater-surface water exchange flow patterns by streambed temperature anomalies

The time-series of the temperature data revealed substantial differences between groundwater and river temperature dynamics. The temperature difference between groundwater and surface water in the period until the end of August 2009 (up to 9 °C) provided a distinctive signal for tracing the exchange between the water sources at the aquifer-river interface (Fig. 5b).

The FO-DTS temperature monitoring within the sediment identified distinct cold spots along the streambed, indicating distinct up-welling patterns of colder groundwater (Fig. 7). In contrast to previous FO-DTS applications, which identified step functional changes of surface water column bottom temperatures caused by the warming/cooling effect of up-welling groundwater (Selker et al., 2006; Westhoff et al., 2007),

HESSD
9, 337–378, 2012

temperatures at the sediment surface did not vary by more than >0.05 °C along the stream reach. In our study FO-DTS monitored cold spots in streambed temperatures were defined by discrete anomalies, indicating that groundwater up-welling reduced streambed temperatures only locally (Fig. 7).

Although the signal strength $A_T(x_i)$ determined by the range of local streambed temperature deviations from the spatial average, varied slightly throughout different observation dates, spatial temperature patterns remained constant and, therefore, seem to provide a robust indicator of groundwater up-welling locations (Fig. 8b). Persistently colder streambed temperatures were identified as groundwater up-welling hotspots at the most up-stream and down-stream sections (P1–3; P25–27) as well as at locations around piezometer P4, P8 and P12, whereas 2–2.3 °C higher temperatures for the rest of the river reach indicated no groundwater up-welling. Furthermore, as the temperature anomaly patterns prove to be temporally persistent, the same can be assumed for the locations of increased groundwater inflow, at least over the time scale of the summer months of 2009. The high temporal variability at locations with strong temperature anomalies is likely to result from variable groundwater upwelling causing a range of mixing temperatures.

With up to 1.8 °C of spatial variation between suspected up-welling and non-up-welling locations the signal strength is significantly higher (>5 times) than topography-driven temperature variability at the streambed surface. This has been identified not to exceed 0.3 °C in a previous study (Krause et al., 2011b) and is, therefore, likely to cause only minor uncertainty in the FO-DTS data interpretation. It is important to note that the effects of solar radiation and shading on the streambed temperatures can be excluded as the stream flow velocities of persistently >0.4 m s^{-1}, average water depths of 0.5–1.5 m and discharges of $Q > 0.5$ m^3 s^{-1} during the observation period would prevent the shading-related cooling as well as direct radiation induced preferential heating of the bottom of the water column.

HESSD
9, 337–378, 2012

4.3 Synthesis: conjunctive interpretation of VHG and temperature information for identifying exchange flow patterns in dependence of aquifer-river connectivity

While FO-DTS observed streambed temperature distributions represent a powerful indicator of groundwater up-welling, they do not provide an insight into why the groundwater is up-welling at distinct locations. However, by combining DTS-derived streambed temperatures with VHGs, further insights into the nature and streambed controls on groundwater-surface water exchange in the investigated lowland stream section can be obtained.

4.3.1 A framework for process inference

For summer conditions in groundwater gaining streams we suggest the following framework of process inferences: High hydraulic fluxes can result either from high pressure gradients or high permeabilities. Under conditions where strong cold temperature anomalies suggest high groundwater inflow, it can be assumed that the coincidence of high VHG with strong streambed temperature anomalies indicates intensive groundwater up-welling (*CASE 1*). Such conditions might particularly be encountered at locations of preferential pressure release through highly conductive sediments adjacent to flow confining streambed structures. Alternatively, the occurrence of low VHG and small streambed temperature anomalies indicates locations of no or reduced groundwater up-welling (*CASE 2*) which could result from these areas being bypassed by the regionally up-welling groundwater (e.g. due to preferential lateral flow) or flow confining streambed structures beneath the zone of investigations. However, if high VHG anomalies do not coincide with strong temperature anomalies this indicates that up-welling pressure gradients exist but the flow is locally inhibited by low conductivity streambed sediments (*CASE 3*). In contrast, low VHG anomalies at locations with strong streambed temperature anomalies can indicate groundwater up-welling through highly conductive streambed sediments (*CASE 4*).

HESSD
9, 337–378, 2012

4.3.2 Application and validation of the framework

In the research area, *CASE 4* conditions can be found at the P1–2 and P25–27 northern/southern ends of the reach, where significant temperature differences from the spatial average (Fig. 9c) coincide with generally low to moderate VHG anomalies (Fig. 9d), indicating strong groundwater up-welling through moderate to highly conductive streambed sediments. At these locations, similar to piezometer locations P6–7, P10–11, P13–17 and P24 which represent characteristic *CASE 2* conditions with low deviation from spatial average temperatures (Fig. 9c) and VHG's (Fig. 9d), no flow confining structures have been detected along the streambed piezometers (Table 2). In contrast, the moderate-to-high VHG anomalies around piezometer P5, P9, P18–19 and section P21–23 (Figs. 6 and 9d), which do not exhibit significant streambed temperature anomalies (Fig. 9c), indicate up-welling inhibition by confining streambed sediments (corresponding with *CASE 3* conditions). This interpretation is confirmed by the observation of flow confining streambed layers in piezometers P5, P9, P18, P19, P21, P22, P23 (Table 2, Fig. 6). In particular around piezometers P3, P4, P8 and P12, which represent locations without flow confining sediment structures but within close vicinity to identified low conductivity sediments (Table 2) high VHG anomalies (Fig. 9d) coincide with high temperature anomalies (Fig. 9c), indicating *CASE 1* conditions with intensive up-welling along preferential pressure release flow paths.

As already suggested by Fig. 9a, the temporal variability (STDEV) in the temperature signal strength $A_T(x_i)$ is generally larger at locations of high temperature anomalies where local temperatures were below the spatial average (Fig. 9e). It also appears that piezometers close to FO-DTS indicated up-welling locations (high $A_T(x_i)$) are characterised by lower temporal variability (STDEV) of $A_{\mathrm{VHG}}(x_i)$) (Fig. 9f). This supports the hypothesis that high temporal variability of VHG anomalies $A_{\mathrm{VHG}}(x_i)$ is more closely connected to up-welling inhibition by low permeability barriers (see Sect. 4.1) than with groundwater influx into the river. This assumption is confirmed by the observation that

HESSD
9, 337–378, 2012

at locations with up-welling inhibition highest VHG anomalies $A_{VHG}(x_i)$ coincide with high STDEV in signal strength (Fig. 9b).

4.3.3 Uncertainties and limitations in transferability of the framework to other flow systems

The presented approach is tested in this study for summer baseflow conditions in a groundwater gaining lowland stream. Although adaptations of the approach are expected to be transferable to different systems, its applicability for other conditions requires further validation. Patterns and dynamics of temperature and VHG anomalies will be different for instance for winter conditions (with inverse temperature gradients) as well as loosing stream reaches with negative VHG gradients. For example, in case of a river with similar groundwater-surface water thermal gradients, a low streambed permeability with only a few locations where the stream was losing water, temperature anomalies might be warm (in summer) combined with a higher variability of the strength of the anomaly. Temperature fluctuations in this case would not only result from conduction but also from advection, and the temperature signal would, hence be controlled by (a) the surface water temperature variability and (b) the fluctuation in hydraulic gradients).

The presented methodology based on streambed temperature patterns by FO-DTS, strongly relies on the ability to correctly deploy the cable within the streambed sediments. At locations, where field conditions prevent the installation of fibre-optic cables within the streambed, the applicability of the presented approach might be limited. In particular in environments with small relative groundwater contributions to the stream discharge, the groundwater temperature signal is likely to attenuate very quickly within the surface water column. Potential future applications of the presented approach in different environmental settings will need to ensure that more pronounced diurnal surface water temperature amplitudes or preferential heating/shading of the streambed do not critically interfere with the application of temperature as a tracer of aquifer-river exchange flow patterns.

HESSD
9, 337–378, 2012

5 Conclusions

The results of this study demonstrate the potential of FO-DTS observations along a fibre-optic cable buried in the streambed for tracing complex patterns of exchange fluxes across the aquifer-river interface of larger lowland rivers with proportionally smaller groundwater contributions to the overall discharge. FO-DTS monitored temperature patterns in the research area revealed distinct up-welling hotspots in the streambed. In contrast to a number of previous FO-DTS applications predominantly in headwater streams, which found up-welling groundwater to effect bottom temperatures of the surface water column that propagated downstream, groundwater contributions in the investigated stream section did only cause local, spatially very discrete temperature anomalies within the streambed and did not influence temperatures further downstream. The results of this study provide strong evidence for the advantage of FO-DTS monitoring in such systems, as traditional roaming temperature surveys of larger areas or a limited number of temperature profiles in the streambed sediments have a high probability of not capturing the very distinct and localized hotspots of groundwater inflow.

Although VHG patterns in the streambed are not suitable for directly determining groundwater-surface water exchange fluxes, when combined with FO-DTS observations of streambed temperature anomalies, they proved a useful indicator for the discrimination of driving forces and inhibitors of exchange over the aquifer-river interface. The comparison of patterns in VHG and FO-DTS derived temperature deviations from their spatial averages provides a powerful framework for the conclusive identification of aquifer-river exchange fluxes in dependence of streambed hydraulic conductivity patterns. Our results illustrate the value of combined data sets of FO-DTS sampled temperature patterns and VHG observations for improving the understanding of controls and dynamics of groundwater-surface water exchange fluxes in lowland rivers with complex small-scale streambed transmissivity patterns in particular when information of structural streambed heterogeneity is limited. By using comparative FO-DTS

HESSD
9, 337–378, 2012

and VHG observations as hypotheses testing tool, this study furthermore provides a successfully validated strategy for the application of FO-DTS surveys to optimise the experimental design of future investigations in lowland river streambeds.

The presented approach has in this study been validated for summer baseflow conditions in lowland rivers where discharge of cold groundwater causes anomalies in streambed temperature patterns and vertical hydraulic gradients. Future research should focus on testing the applicability of the presented methodology and adapting it for contrasting streambed environments, including winter conditions (with inverse temperature gradients) and loosing streams.

Acknowledgements. The authors wish to acknowledge support of the presented work by the Royal Geographical Society, EPSRC and NERC (NE/I016120). We would also like to thank Fred Day-Lewis (USGS) for the kind provision of the FO-DTS mapping scripts, Kevin Voyce (Environment Agency of England and Wales) for hydro-meteorological data and Emma Naden (University of Keele), Christina Tecklenburg and Mathias Munz (University of Potsdam) for fieldwork support.

References

Anderson, M. P.: Heat as a Ground Water Tracer, Ground Water, 43, 951–968, 2005.

Anibas, C., Fleckenstein, J. H., Volze, N., Buis, K., Verhoeven, R., Meire, P., and Batelaan, O.: Transient or Steady-state? Using vertical temperature profiles to quantify groundwater-surface water exchange, Hydrol. Process., 23, 2165–2177. 2009.

Bencala, K. E.: A perspective on stream-catchment connections, J. N. Am. Benthol. Soc., 12, 44–47, 1993.

Boano, F., Camporeale, C., Revelli, R., and Ridolfi, L.: Sinuosity-driven hyporheic exchange in meandering rivers, Geophys. Res. Lett., 33, 1–4, 2006.

Boano, F., Demaria, A., Revelli, R., and Ridolfi, L.: Biogeochemical zonation due to intrameander hyporheic flow, Water Resour. Res., 46, W02511, doi:10.1029/2008WR007583, 2010.

Boulton, A. J.: Hyporheic rehabilitation in rivers: restoring vertical connectivity, Freshwater Biol., 52, 632–650, 2007.

HESSD

9, 337–378, 2012

Boulton, A. J., Findlay, S., Marmonier, P., Stanley, E. H., and Valett, H. M.: The functional significance of the hyporheic zone in streams and rivers, Ann. Rev. Ecol. Syst., 29, 59–81, 1998.
Brunke, M. and Gonser, T.: The ecological significance of exchange processes between rivers and groundwater, Freshwater Biol., 37, 1–33, 1997.
Calver, A.: Riverbed permeabilities: Information from pooled data, Ground Water, 39, 546–553, 2001.
Cardenas, M. B.: Stream-aquifer interactions and hyporheic exchange in gaining and losing sinuous streams, Water Resour. Res., 45, W06429, doi:10.1029/2008WR007651, 2009.
Cardenas, M. B. and Wilson, J. L.: The influence of ambient groundwater discharge on exchange zones induced by current-bedform interactions, J. Hydrol., 331, 103–109, 2006.
Cardenas, M. B. and Wilson, J. L.: Thermal regime of dune-covered sediments under gaining and losing water bodies, J. Geophys. Res., 112, G04013, doi:10.1029/2007JG000485, 2007.
Cardenas, M. B., Wilson, J. L., and Zlotnik, V. A.: Impact of heterogeneity bedform configuration, and channel curvature on hyporheic exchange, Water Resour. Res., 40, W08307, doi:10.1029/2004WR003008, 2004.
Cardenas, M. B., Wilson, J. L., and Haggerty, R.: Residence time of bedform-driven hyporheic exchange, Adv. Water Resour., 31, 1382–1386, 2008.
Chafiq, M., Gibert, J., and Claret, C.: Interactions among sediments, organic matter and microbial activity in the hyporheic zone of an intermittent stream, Can. J. Fish. Aquat. Sci., 56, 487–495, 1999.
Conant, B.: Delineating and quantifying ground water discharge zones using streambed temperatures, Ground Water, 42, 243–257, 2004.
Constantz, J.: Heat as a tracer to determine streambed water exchanges: Water Resour. Res., 44, W00D10, doi:10.1029/2008WR006996, 2008.
Constantz, J., Tyler, S. W., and Kwicklis, E.: Temperature-profile methods for estimating percolation rates in arid environments, Vadose Zone J., 2, 12–24, 2003.
Dole-Olivier, M. J., Marmonier, P., and Beffy, J. L.: Response of invertebrates to lotic disturbance: Is the hyporheic zone a patchy refugium?, Freshwater Biol., 37, 257–276, 1997.
Duff, J. H. and Triska, F. J.: Denitrification in the sediments from the hyporheic zone adjacent to a small forested stream, Can. J. Fish. Aquat. Sci., 47, 1140–1147, 1990.

HESSD
9, 337–378, 2012

Duff, J. H. and Triska, F. J.: Nitrogen biochemistry and surface-subsurface exchange in streams, in: Streams and Groundwater, edited by: Jones, J. B. and Mulholland, P. J., Academic Press, London, 197–220, 2000.
Engdahl, N. B., Vogler, E. T., and Weissmann, G. S.: Evaluation of aquifer heterogeneity effects on river flow loss using a transition probability framework, Water Resour. Res., 46, W01506, doi:10.1029/2009WR007903, 2010.
Findlay, S., Strayer, D., Goumbala, C., and Gould, K.: Metabolism of streamwater dissolved organic carbon in the shallow hyporheic zone, Limnol. Oceanogr., 38, 1493–1499, 1993.
Findlay, S. E. G., Sinsabough, R. L., Sobczak, W. V., and Hoostal, M.: Metabolic and structural response of hyporheic microorganisms to variations in supply of dissolved organic matter, Limnol. Oceanogr., 48, 1608–1617, 2003.
Fisher, S. G., Grimm, N. B., Marti, E., Holmes, R. M., and Jones, J. B.: Material spiraling in stream corridors: A telescoping ecosystem model, Ecosystems, 1, 19–34, 1998.
Fleckenstein, J. H., Niswonger, R. G., and Fogg, G. E.: River-aquifer interactions, geologic heterogeneity, and low-flow management, Ground Water, 44, 837–852, 2006.
Frei, S., Fleckenstein, J. H., Kollet, S. J., and Maxwell, R. M.: Patterns and dynamics of river-aquifer exchange with variably-saturated flow using a fully-coupled model, J. Hydrol., 375, 383–393, 2009.
Genereux, D. P., Leahy, S., Mitasova, H., Kennedy, C. D., and Corbett, D. R.: Spatial and temporal variability of streambed hydraulic conductivity in West Bear Creek, North Carolina, USA, J. Hydrol., 358, 332–353, 2008.
Hannah, D. M., Malcolm, I. A., Soulsby, C., and Youngson, A. F.: Heat exchanges and temperatures within a salmon spawning stream in the Cairngorms, Scotland: seasonal and sub-seasonal dynamics, River Res. Appl., 20, 635–652, 2004.
Hannah, D. M., Malcolm, I. A., and Bradley, C.: Seasonal hyporheic temperature dynamics over riffle bedforms, Hydrol. Process., 23, 2178–2194, 2009.
Hatch, C. E., Fisher, A. T., Ruehl, C. R., and Stemler, G.: Spatial and temporal variations in streambed hydraulic conductivity quantified with time-series thermal methods, J. Hydrol., 389, 276–288, doi:10.1016/j.jhydrol.2010.05.046, 2010.
Hill, A. R. and Cardaci, M.: Denitrification and organic carbon availability in riparian wetland soils and subsurface sediments, Soil Sci. Soc. Am. J., 68, 320–325, 2004.

HESSD
9, 337–378, 2012

Hinkle, S. R., Duff, J. H., Triska, F. J., Laenen, A., Gates, E. B., Bencala, K. E., Wentz, D. A., and Silva, S. R.: Linking hyporheic flow and nitrogen cycling near the Willamette River – a large river in Oregon, USA, J. Hydrol., 244, 157–180, 2001.

Jones, J. B., Holmes, R. M., Fisher, S. G., Grimm, N. B., and Greene, D. M.: Methanogenesis In Arizona, Usa Dryland Streams, Biogeochemistry, 31, 155–173, 1995.

Käser, D., Binley, A., Heathwaite, L., and Krause, S.: Spatio-temporal variations of hyporheic flow in a riffle-step-pool sequence, Hydrol. Process., 23, 2138–2149, 2009.

Kasahara, T. and Hill, A. R.: Modeling the effects of lowland stream restoration projects on stream-subsurface water exchange, Ecol. Eng., 32, 310–319, 2008.

Kasahara, T. and Wondzell, S. M.: Geomorphic controls on hyporheic exchange flow in Mountain Streams, Water Resour. Res., 39, 1–14, 2003.

Keery, J., Binley, A., Crook, N., and Smith, J. W. N.: Temporal and spatial variability of groundwater-surface water fluxes: development and application of an analytical method using temperature time series, J. Hydrol., 336, 1–16, 2007.

Krause, S., Heathwaite, A. L., Miller, F., Hulme, P., and Crowe, A.: Groundwater-dependent wetlands in the UK and Ireland: controls, eco-hydrological functions and assessing the likelihood of damage from human activities, J. Water Resour. Manage., 21, 2015–2025, 2008a.

Krause, S., Jacobs, J., Habeck, A., Bronstert, A., and Zehe, E.: Assessing the impact of changes in landuse and management practices on the diffusive pollution and retention of nitrate in a riparian floodplain, Sci. Total Environ., 389, 149–164, 2008b.

Krause, S., Hannah, D. M., and Fleckenstein, J. H.: Hyporheic hydrology: interactions at the groundwater-surface water interface, Hydrol. Process., 23, 2103–2107, 2009a.

Krause, S., Heathwaite, A. L., Binley, A., and Keenan, P.: Nitrate concentration changes along the groundwater – surface water interface of a small Cumbrian river, Hydrol. Process., 23, 2195–2211, 2009b.

Krause, S., Hannah, D. M., Fleckenstein, J. H., Heppell, C. M., Pickup, R., Pinay, G., Robertson, A. L., and Wood, P. J.: Inter-disciplinary perspectives on processes in the hyporheic zone, Ecohydrol. J., 4, 1–19, 2011a.

Krause, S., Hannah, D. M., and Blume, T.: Heat transport patterns at pool-riffle sequences of an UK lowland stream, Ecohydrol. J., 4, 549–563, doi:10.1002/eco.199, 2011b.

Lautz, L. K., Kranes, N. T., and Siegel, D. I.: Heat tracing of heterogeneous hyporheic exchange adjacent to in-stream geomorphic features, Hydrol. Process., 24, 3074–3086, doi:10.1002/hyp.7723, 2010.

HESSD
9, 337–378, 2012

Leek, R., Wu, J. Q., Wang, L., Hanrahan, T. P., Barber, M. E., and Qiu, H.: Heterogeneous characteristics of streambed saturated hydraulic conductivity of the Touchet River, south eastern Washington, USA, Hydrol. Process., 23, 1236–1246, doi:10.1002/hyp.7258, 2009.

Lowry, C. S., Walker, J. F., Hunt, R. J., and Anderson, M. P.: Identifying spatial variability of groundwater discharge in a wetland stream using a distributed temperature sensor, Water Resour. Res., 43, W10408, doi:10.1029/2007WR006145, 2007.

Malard, F., Ferreira, D., Doledec, S., and Ward, J. V.: Influence of groundwater upwelling on the distribution of the hyporheos in a headwater river flood plain, Arch. Hydrobiol., 157, 89–116, 2003.

Malcolm, I. A., Soulsby, C., and Youngson, A. F.: Thermal regime in the hyporheic zone of two contrasting salmonid spawning streams, Fish. Manage. Ecol., 9, 1–10, 2002.

Malcolm, I. A., Soulsby, C., Youngson, A. F., Hannah, D. M., McLaren, I. S., and Thorne, A.: Hydrological influences on hyporheic water quality: implications for salmon survival, Hydrol. Process., 18, 1543–1560, 2004.

Mulholland, P. J., Tank, J. L., Sanzone, D. M., Wollheim, W. M., Peterson, B. J., Webster, J. R., and Meyer, J. L.: Nitrogen cycling in a forest stream determined by a 15 N tracer addition., Ecol. Monogr., 70, 471–493, 2000.

Mulholland, P. J., Helton, A. M., Poole, G. C., Hall, R. O., Hamilton, S. K., Peterson, B .J., Tank, J. L., Ashkenas, L. R., Cooper, L. W., Dahm, C. N., Dodds, W. K., Findlay, S. E. G., Gregory, S. V., Grimm, N. D., Johnson, S. L., McDowell, W. H., Meyer, J. L., Valett, H. M., Webster, J. R., Arango, C. P., Beaulieu, J. J., Bernot, M. J., Burgin, A. J., Crenshaw, C. L., Johson, L. T., Niederlehner, B. R., O'Brien, J. M., Potter, J. D., Sheibley, R. W., Sobota, D. J., and Thomas, S. M.: Stream denitification across biomes and its response to anthropogenic nitrate loading, Nature, 452, 202–205, 2008.

Pinay, G., O'Keefe, T. C., Edwards, R. T., and Naiman, R. J.: Nitrate removal in the hyporheic zone of a salmon river in Alaska, River Res. Appl., 25, 367–375, 2009.

Robertson, A. L. and Wood, P. J.: Ecology of the hyporheic zone: origins, current knowledge and future directions, Fundament. Appl. Limnol., 176, 277–289, 2010.

Rosenberry, D. O.: A seepage meter designed for use in flowing water, J. Hydrol., 359, 118–130, 2008.

Rosenberry, D. O. and Pitlick, J.: Local-scale spatial and temporal variability of seepage in a shallow gravel-bed river, Hydrol. Process., 23, 3306–3318, 2009.

HESSD
9, 337–378, 2012

Schmidt, C., Conant, B., Bayer-Raich, M., and Schirmer, M.: Evaluation and field-scale application of an analytical method to quantify groundwater discharge using mapped streambed temperatures, J. Hydrol., 347, 292–307, 2007.
Selker, J., van de Giesen, N., Westhoff, M., Luxemburg, W., and Parlange, M. B.: Fiber optics opens window on stream dynamics, Geophys. Res. Lett., 33, L24401, doi:10.1029/2006GL027979, 2006.
Selker, J. S.: Taking the temperature of ecological systems with fibre-optics, EOS Trans. AGU, 89, 187, 2008.
Slater, L. D., Ntarlagiannis, D., Day-Lewis, F. D., Mwakanyamale, K., Versteeg, R. J., Ward, A., Strickland, C., Johnson, C. D., and Lane Jr., J. W.: Use of electrical imaging and distributed temperature sensing methods to characterize surface water – groundwater exchange regulating uranium transport at the Hanford 300 Area, Washington, Water Resour. Res., 46, W10533, doi:10.1029/2010WR009110, 2010.
Sophocleous, M.: Interactions between groundwater and surface water: the state of science, Hydrogeol. J., 10, 52–67, 2002.
Storey, R. G., Howard, K. W. F., and Williams, D. D.: Factors controlling rifflescale hyporheic exchange flows and their seasonal changes in a gaining stream: A three dimensional groundwater flow model, Water Resour. Res., 39, 1034, 8-1–8-17, 2003.
Storey, R. G., Williams, D. D., and Fulthorpe, R. R.: Nitrogen Processing In The Hyporheic Zone Of A Pastoral Stream, Biogeochemistry, 69, 285–313, 2004.
Stubbington, R., Wood, P. J., and Boulton, A. J.: Low flow controls on benthic and hyporheic macroinvertebrate assemblages during a supra-seasonal drought, Hydrol. Process., 23, 2252–2264, 2009.
Tonina, D. and Buffington, J. M.: Hyporheic exchange in gravel bed rivers with pool-riffle morphology: laboratory experiments and three-dimensional modelling, Water Resour. Res., 43, W01421, doi:10.1029/2005WR004328, 2007.
Tyler, S. W., Selker, J. S., Hausner, M. B., Hatch, C. E., Torgersen, T., Thodal, C. E., and Schladow, S. G.: Environmental temperature sensing using Raman spectra DTS fiber-optic methods, Water Resour. Res., 45, W00D23, doi:10.1029/2008WR007052, 2009.
Webb, B. W., Hannah, D. M., Moore, R. D., Brown, L. E., and Nobilis, F.: Recent advances in stream and river temperature research, Hydrol. Process., 22, 902–918, 2008.
Weight, W.: Hydrogeology Field Manual, 2nd Edn., McGraw-Hill Professional, p.751, 2008.

HESSD
9, 337–378, 2012

Westhoff, M. C., Savenije, H. H. G., Luxemburg, W. M. J., Stelling, G. S., van de Giesen, N. C., Selker, J. S., Pfister, L., and Uhlenbrook, S.: A distributed stream temperature model using high resolution temperature observations, Hydrol. Earth Syst. Sci., 11, 1469–1480, doi:10.5194/hess-11-1469-2007, 2007.

White, D. S.: Perspectives on defining and delineatinghyporheic zones. J. N. Am. Benthol. Soc., 12, 61–69, 1993.

Woessner, W. W.: Stream and fluvial plain ground water interactions: rescaling hydrogeologic thought, Ground Water, 38, 423–429, 2000.

Wondzell, S. M.: Effect of morphology and discharge on hyporheic exchange flows in two small streams in the Cascade Mountains of Oregon, USA, Hydrol. Process., 20, 267–287, 2006.

Zarnetske, J. P., Haggerty, R., Wondzell, S. M., and Baker, M. A.: Labile Dissolved Organic Carbon Supply Controls Hyporheic Denitrification, J. Geophys. Res., 116, G04036, doi:10.1029/2011JG001730, 2011a.

Zarnetske, J. P., Haggerty, R., Wondzell, M., and Baker, M. A.: Dynamics of nitrate production and removal as a function of residence time in the hyporheic zone, J. Geophys. Res., 116, G01025, doi:10.1029/2010JG001356, 2011b.

HESSD
9, 337–378, 2012

Table 1. Spatial and temporal resolution of environmental parameters monitored during the 2009 sampling period.

Environmental Variable	Observation interval	Instrumentation	Accuracy
Temperature – SW Temperature – GW	5 min 15 min	Solinst LT M5/F15 diver, combined level and temperature logger	±0.05 °C ±0.05 °C
Temperature – HZ	15 min	Hobo – 4-channel temperature logger and thermocouple sensors	±0.025°C
Temperature – Air	1 h	Keele, meteorological station	±0.05°C
Hydraulic head – SW/Hydraulic head – GW/ Barometric head	5 min/15 min/ 5 min	Solinst LT M5/F15 diver, combined water level and temperature logger/ Solinst BaroLogger	±0.3 cm
Hydraulic head streambed surveys 2009	21/05, 02/06, 19/06, 30/06, 31/07, 21/08, 30/09	Streambed piezometer and meteorological graduated dip-meter	±0.3 cm
Precipitation	1 h	Keele, station (18 km distance)	±0.2 mm
Discharge (Q)	1 h	EA gauging station Tern Hill	±5 %
DTS streambed temperature surveys 2009	23/07, 03/08, 06/08, 18/08, 19/08 (night), 19/08 (day)	FO-DTS (Sensornet Halo)	±0.05 °C

HESSD
9, 337–378, 2012

Table 2. Average differences to spatial mean in VHG and DTS monitored streambed temperatures over the entire VHG and DTS survey period in comparison to streambed structural information of up-welling inhibition. Case distinction of VHG vs. DTS deviations from mean: *CASE 1* = white, *CASE 2* = yellow, *CASE 3* = red, *CASE 4* = green.

Piezometer ID	VHG – difference to spatial mean	DTS – difference to spatial mean (nearest)	Flow confinement (*y*/*n*)
T1	−0.013	−0.59	No
T2	−0.004	−0.25	No
T3	0.023	−0.27	No
T4	0.085	−0.16	No
T5	−0.007	+0.21	Yes (75 cm)
T6	−0.076	+0.20	No
T7	−0.063	+0.21	No
T8	0.175	−0.35	No
T9	0.022	0.26	Yes (100 cm)
T10	−0.031	0.24	Yes (125 cm)
T11	−0.087	0.21	No
T12	0.071	−0.69	No
T13	−0.149	0.10	No
T14	−0.130	−0.11	No
T15	0.029	0.10	No
T16	−0.050	0.10	No
T17	−0.242	0.05	No
T18	0.145	0.12	Yes (50–75 cm)
T19	0.297	0	Yes (75 cm)
T20	−0.196	0.10	No
T21	0.029	0.12	Yes (100–120 cm)
T22	0.120	0.05	Yes (75–125 cm)
T23	0.186	0.26	Yes (75 cm)
T24	−0.018	0.08	No
T25	−0.037	−0.72	No
T26	−0.034	−0.28	No
T27	−0.082	−0.82	No

HESSD
9, 337–378, 2012

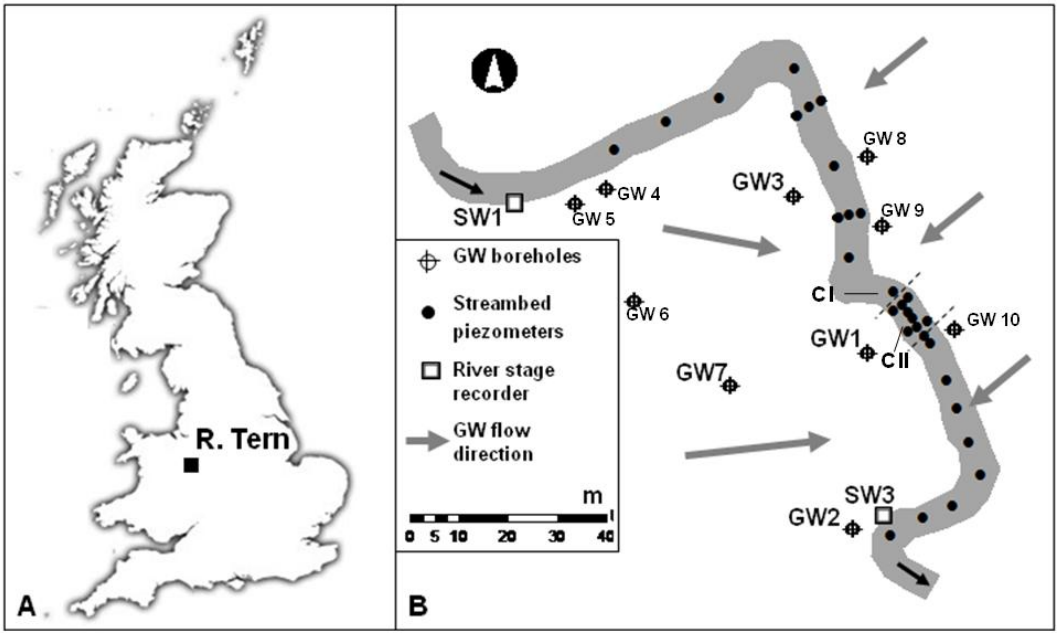

Fig. 1. **(A)** Fieldsite location in the UK and **(B)** experimental design at the River Tern with groundwater boreholes (GW), surface water gauges (SW) and the streambed piezometer network. The location of exemplary sediment cores CI and CII are also indicated.

HESSD
9, 337–378, 2012

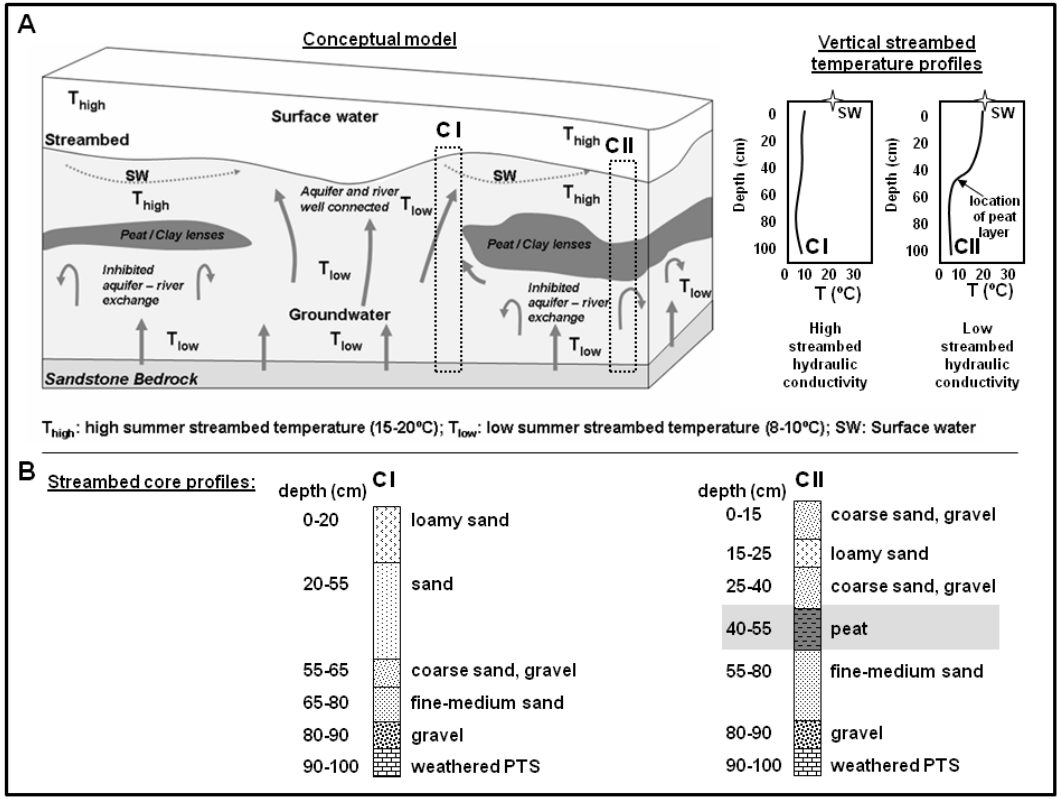

Fig. 2. (A) Conceptual model of streambed hydrofacies controlling groundwater up-welling in a typical lowland river including their effect on heat transport at the aquifer-river interface (the star indicates the temperature of the surface water). **(B)** Core logs of exemplary streambed cores (for sampling locations see Fig. 1).

HESSD
9, 337–378, 2012

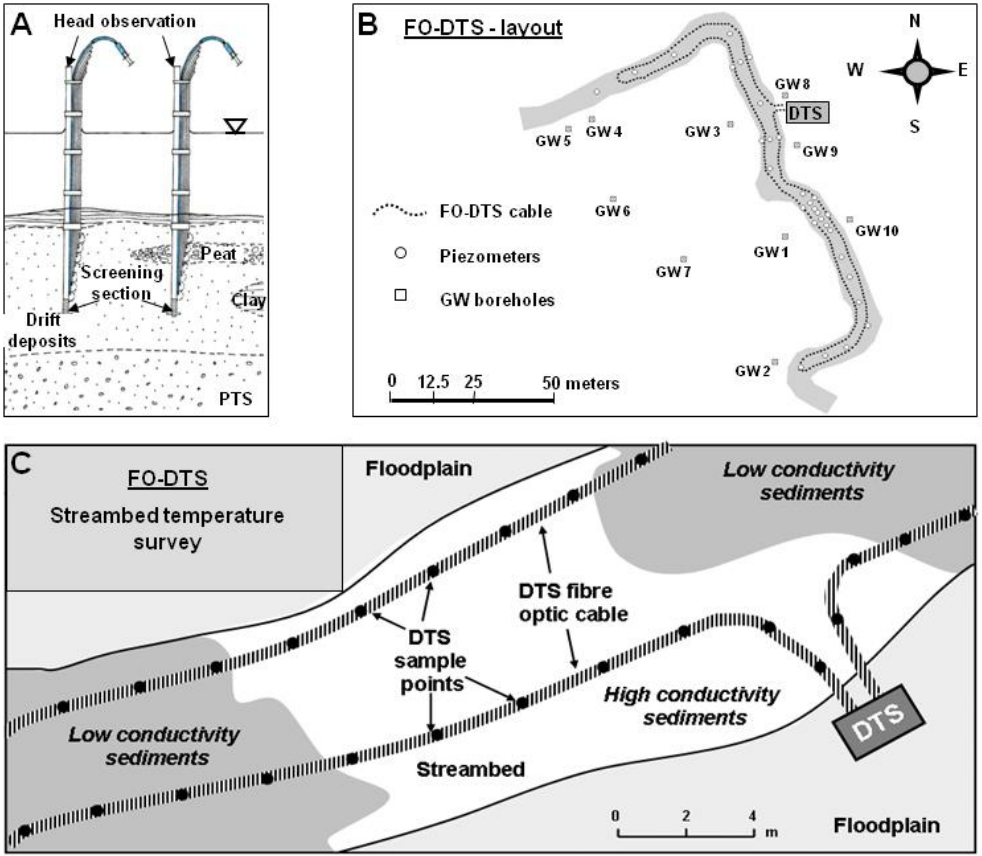

Fig. 3. Experimental installations at the River Tern with **(A)** streambed piezometer setup for VHG monitoring, PTS = Permo-Triassic Sandstone. **(B)** FO-DTS cable loop in the investigated meander bend; **(C)** close-up of cable layout in the streambed sediment. (The outline of the low-conductivity sediments is hypothetical.)

HESSD
9, 337–378, 2012

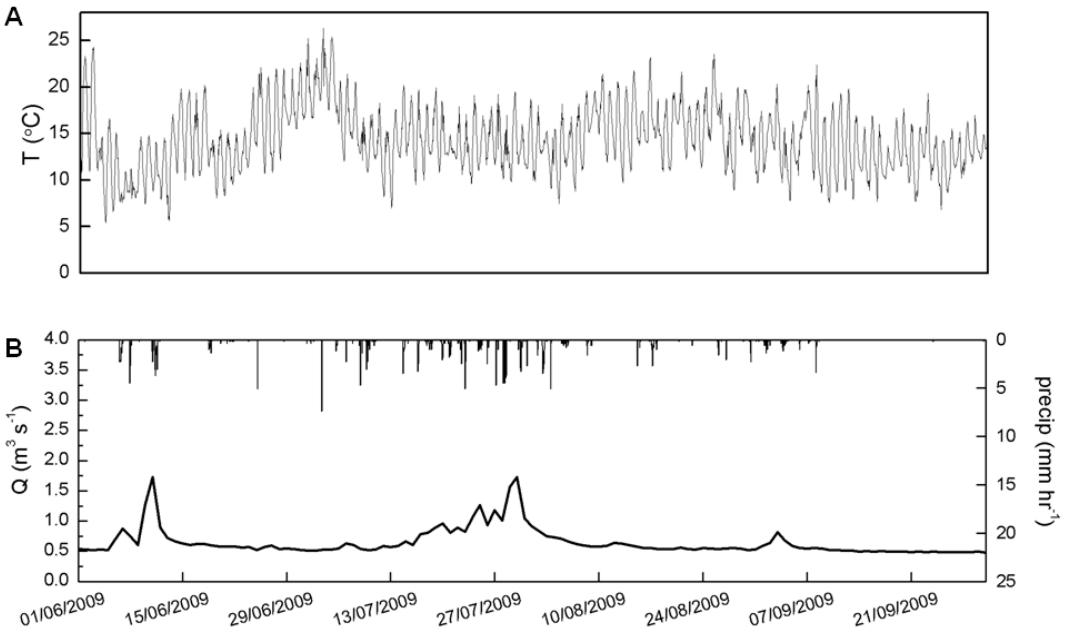

Fig. 4. Hydrometeorological conditions at the fieldsite **(A)** air temperatures, **(B)** precipitation and river discharge (EA Tern Hill gauging station) for the period of 1 June 2009–30 September 2009.

HESSD
9, 337–378, 2012

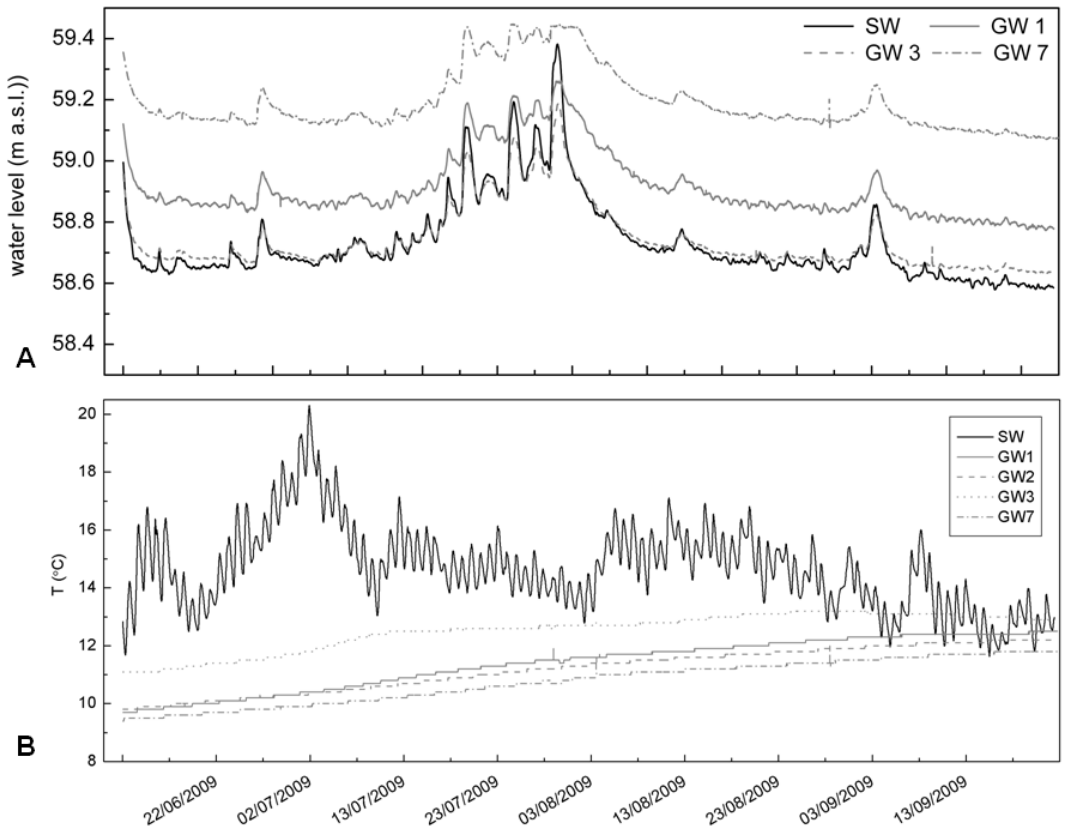

Fig. 5. (A) Surface water levels (SW3, Fig. 1b) and groundwater heads measured at representative locations shown in Fig. 1 for the period of 1 June 2009–30 September 2009. **(B)** Surface water and groundwater temperatures at the locations shown in Fig. 1 for the period of 1 June 2009–30 September 2009.

HESSD
9, 337–378, 2012

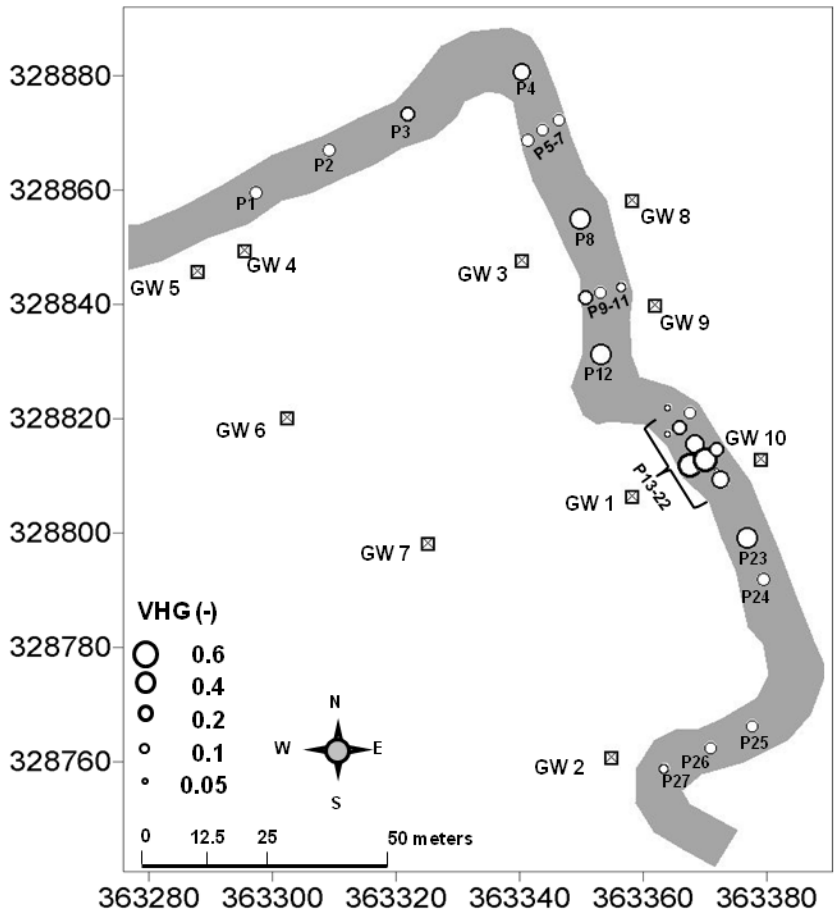

Fig. 6. Spatial patterns of average vertical hydraulic gradients at streambed piezometers (*P*) for 7 sampling dates between 25 May–30 September 2009 (see Table 1 for the exact dates).

HESSD
9, 337–378, 2012

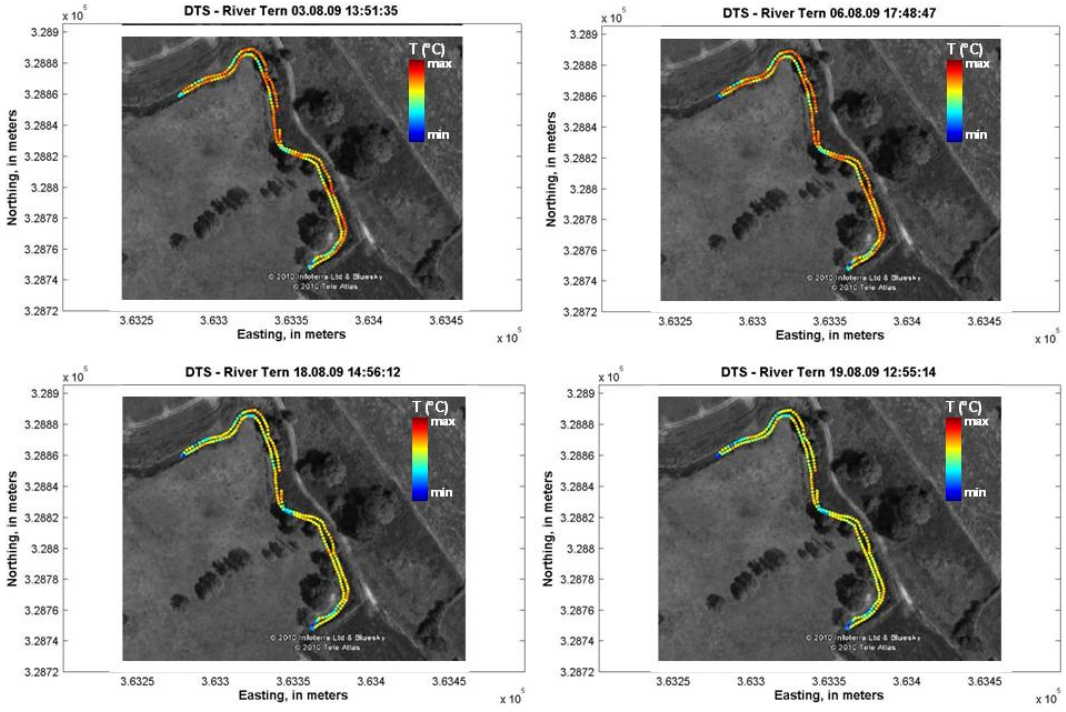

Fig. 7. Spatial patterns streambed temperature anomalies measured with FO-DTS on 4 representative sampling dates in August 2009. The colour scheme covers a range of 3 °C for all 4 maps (absolute temperatures varied slightly from one sampling date to the other).

HESSD
9, 337–378, 2012

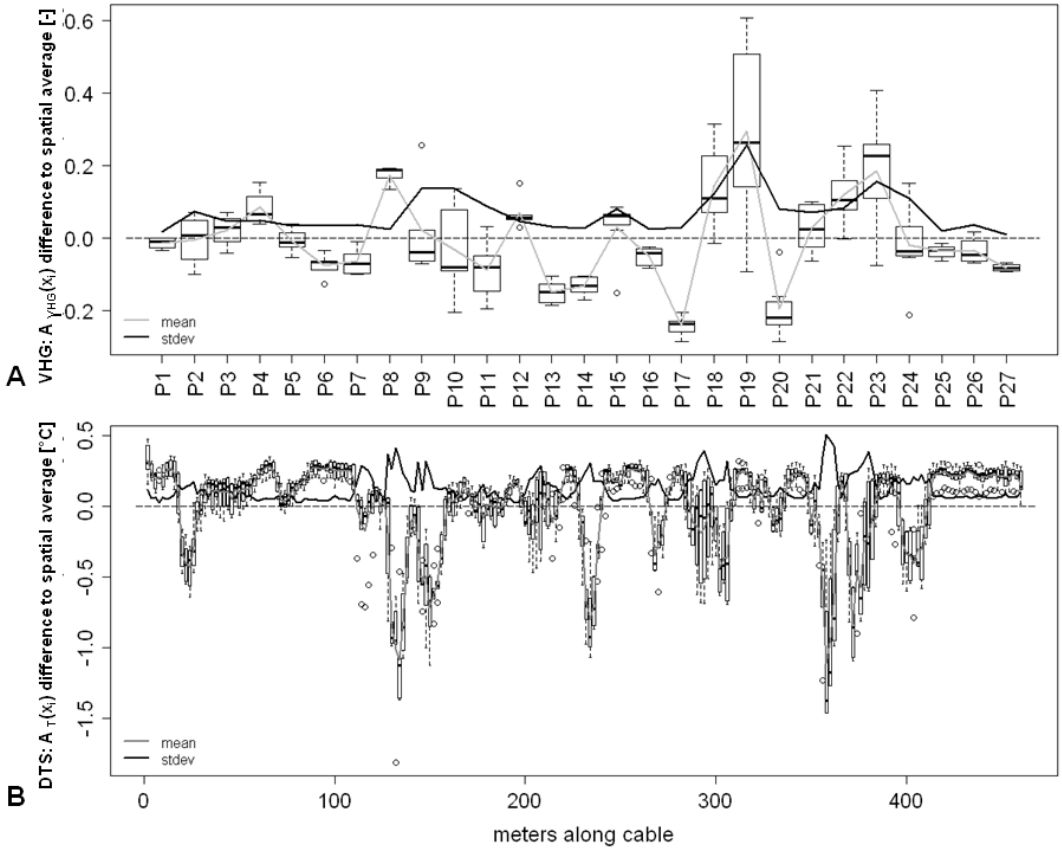

Fig. 8. (A) Box-plots of the temporal and spatial variability of vertical hydraulic gradients along the river reach (north to south) for 4–7 dates (depending on location). Values are standardized by subtracting the spatial mean at each sampling date. **(B)** Box-plots of the temporal and spatial variability of FO-DTS monitored temperatures along the fibre optic cable for all sampling dates. Values are standardized by subtracting the spatial mean at each sampling date.

HESSD
9, 337–378, 2012

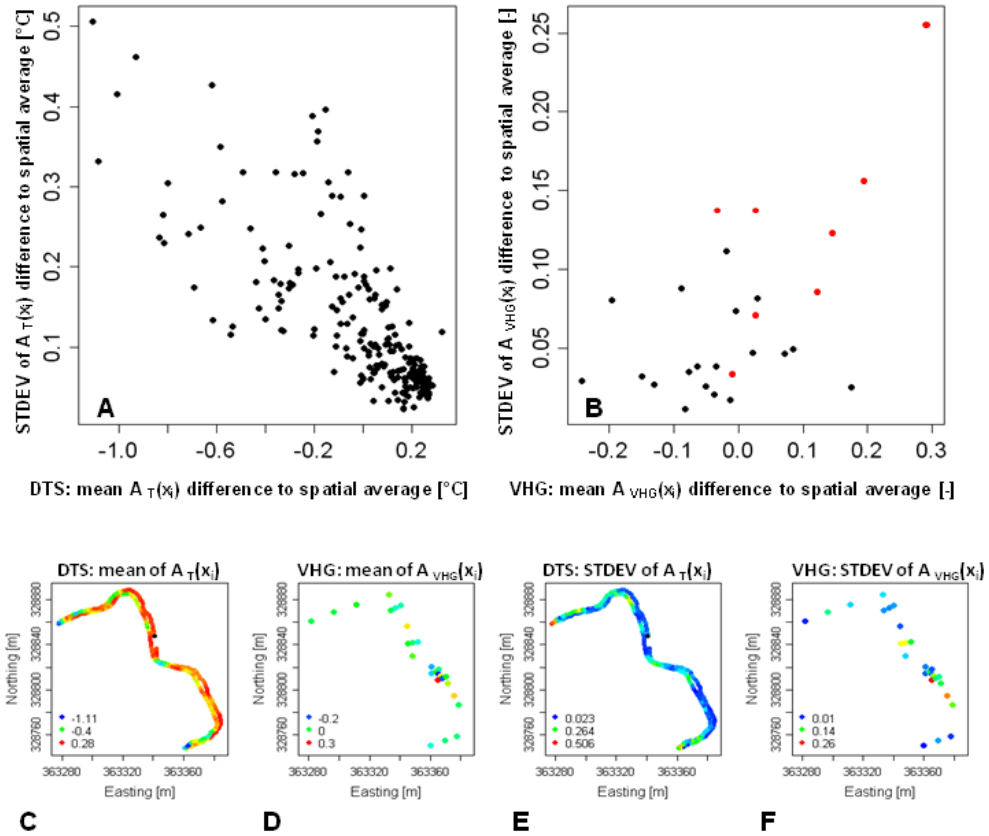

Fig. 9. Comparison of the temporal mean and standard deviation of signal strength for FO-DTS $A_T(x_i)$ **(A)** and VHG $A_{\mathrm{VHG}}(x_i)$ **(B)**. Red symbols indicate piezometers at locations with low conductivity flow confining streambed sediments. Maps of the temporal mean of $A_T(x_i)$ and $A_{\mathrm{VHG}}(x_i)$ for the FO-DTS and the VHG observations **(C, D)** and maps of the corresponding standard deviations of $A_T(x_i)$ and $A_{\mathrm{VHG}}(x_i)$ over all sampling dates **(E, F)**.

HESSD
9, 337–378, 2012